Application of Laser Postionization Secondary Neutral Mass Spectrometry/ Time-of-Flight Secondary Ion Mass Spectrometry in Nanotoxicology: Visualization of Nanosilver in Human Macrophages and Cellular Responses

Andrea Haase,[#,†,*] Heinrich F. Arlinghaus,[#,‡] Jutta Tentschert,[†] Harald Jungnickel,[†] Philipp Graf,[§] Alexandre Mantion,[⊥] Felix Draude,[‡] Sebastian Galla,[‡] Johanna Plendl,[¶] Mario E. Goetz,[†] Admir Masic,[▽] Wolfgang Meier,[§] Andreas F. Thünemann,[⊥] Andreas Taubert,[▽,◆] and Andreas Luch[†,*]

[†]German Federal Institute for Risk Assessment (BfR), Department of Product Safety, Thielallee 88-92, 14195 Berlin, Germany, [‡]Institute of Physics, University of Münster, Wilhelm Klemm Strasse 10, 48149 Münster, Germany, [§]Department of Chemistry, University of Basel, Klingelbergstrasse 80, 4056 Basel, Switzerland, [⊥]BAM, Federal Institute for Materials Research and Testing, Richard-Willstätter-Strasse 11, 12489 Berlin, Germany, [¶]Department of Veterinary Medicine, Institute of Veterinary Anatomy, Free University of Berlin, Koserstrasse 20, 14195 Berlin, Germany, [▽]Max-Planck-Institute of Colloids and Interfaces, Am Mühlenberg 1, 14476 Potsdam-Golm, Germany, and [◆]Institute of Chemistry, University of Potsdam, Karl-Liebknecht-Strasse 24-25, 14476 Potsdam-Golm, Germany. [#] These authors contributed equally to this work.

ABSTRACT Silver nanoparticles (SNP) are the subject of worldwide commercialization because of their antimicrobial effects. Yet only little data on their mode of action exist. Further, only few techniques allow for visualization and quantification of unlabeled nanoparticles inside cells. To study SNP of different sizes and coatings within human macrophages, we introduce a novel laser postionization secondary neutral mass spectrometry (Laser-SNMS) approach and prove this method superior to the widely applied confocal Raman and transmission electron microscopy. With time-of-flight secondary ion mass spectrometry (TOF-SIMS) we further demonstrate characteristic fingerprints in the lipid pattern of the cellular membrane indicative of oxidative stress and membrane fluidity changes. Increases of protein carbonyl and heme oxygenase-1 levels in treated cells confirm the presence of oxidative stress biochemically. Intriguingly, affected phagocytosis reveals as highly sensitive end point of SNP-mediated adversity in macrophages. The cellular responses monitored are hierarchically linked, but follow individual kinetics and are partially reversible.

KEYWORDS: nanosilver · Laser-SNMS · TOF-SIMS · confocal Raman microscopy · oxidative stress · protein carbonyls

Because of their unique physicochemical characteristics and features nanoparticles have been the subject of rapid growth in commercial interest during recent years. Nanosilver belongs to the group of highly commercialized nanomaterials.[1] In the medical field it is used for wound disinfection and sterile coating of surgical instruments. Consumers can be exposed *via* cosmetics or textiles. Nanosilver is also applied as coating material in household devices. At the same time while nanoproducts begin to flood the market and the benefits of nanotechnology receive tremendous attention, unusual and often unpredictable properties of nanomaterials are boosting concerns about possible adverse health effects.[2] Currently risk assessment of nanoparticles is still not reliably feasible and debates are ongoing.

There is little knowledge on tissue barrier penetration and toxicity of silver nanoparticles (SNP). Contrasting the results obtained with nanoscaled titanium dioxide or zinc oxide,[3] nanosilver might well be capable of penetrating human skin.[4] Furthermore, exposure of rats to SNP *via* inhalation or subcutaneous injection results in the uptake and systemic distribution toward different organs including liver and brain.[5] Although the total particle flux might be considered rather low, and *in vivo* studies lack any sign of overt toxicity, supposable internal body exposure to nanosilver demands further studies on acute and long-term effects. Oxidative stress responses are described in cells *in vitro*, but mechanistic details remain elusive.[6] It is known that particle toxicity also depends on physicochemical parameters such as size and surface,[7] yet published data are still inconsistent. A major reason for the limited reproducibility and comparability of studies with SNP

* Address correspondence to andrea.haase@bfr.bund.de, andreas.luch@bfr.bund.de.

Received for review January 16, 2011 and accepted March 23, 2011.

Published online April 02, 2011
10.1021/nn200163w

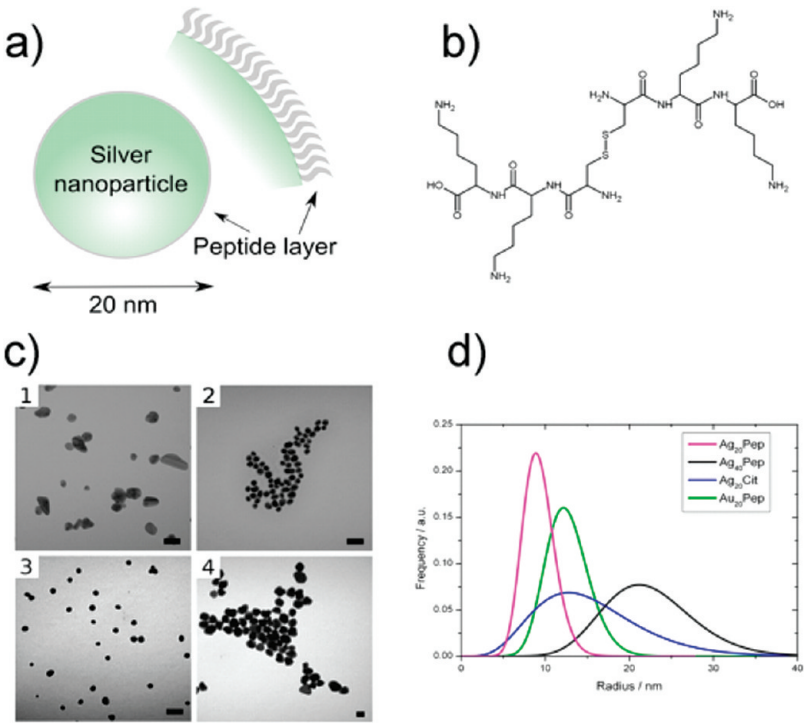

Figure 1. Characterization of nanoparticles. (a) Schematic description of peptide-coated SNP. (b) Sequence and structure of the peptide $(CKK)_2$ used for coating. (c) Representative TEM images of citrate-coated 20 nm silver nanoparticles (Ag_{20}Cit, 1), peptide-coated 20 nm gold nanoparticles (Au_{20}Pep, 2), peptide-coated 20 nm silver nanoparticles (Ag_{20}Pep, 3), and peptide-coated 40 nm silver nanoparticles (Ag_{40}Pep, 4). (d) Polydispersity curves of the nanoparticles applied in our study obtained *via* SAXS measurements (*cf.* Supporting Information, Figure S1).

is the broad diversity in particle sizes, shapes, and coatings. Data on particle characterization are often incomplete and classical approaches of nanosilver synthesis, such as citrate reduction, usually result in broad particle size distribution and significant batch-to-batch variation. For biological studies well-defined particles are mandatory though.

One of the central goals in material sciences lies in the tight control of particle sizes and shapes and in the reproducible production of stable and monodispersed aqueous suspensions. Since they can serve as efficient structure-directing agents working under mild conditions in terms of pH, temperature or solvents, small peptides and proteins currently gain high attention as growth control agents and stabilizers.[8,9] Such biomimetic approaches are highly desirable compared to classic synthesis routes where remaining organic solvents are likely to cause problems in biological applications. Moreover peptide-based synthesis approaches can afford complex bioinorganic hybrid materials with metal cores surrounded by a peptide coat, the latter being advantageous for purification and bioimaging, or as biointerface to control biokinetics and uptake into cells.[8]

One of the major obstacles in the field of nanotoxicology is the lack of reliable and easy-to-perform methods to visualize and quantify nanoparticles inside cells or tissues for assessing internal exposure. Usually transmission electron microscopy (TEM) imaging is used to analyze intracellular particle distribution at very high resolution, but this is time-consuming and requires tedious sample preparation. In terms of 3D reconstruction and quantification it is not straightforward, either.[10] Several microscopic techniques for quantitative and 3D assessment exist but they rely on specifically labeled particles. Major drawbacks are unequal distribution of the fluorescent dye, label-induced alteration of particle properties, or dye leakage. Here we compare several techniques capable of visualizing nanoparticles inside cells without any additional labeling. Because of the covalently linked peptide coat of our SNP[9] we could apply confocal Raman microscopy. In addition we used laser postionization secondary neutral mass spectrometry (Laser-SNMS) and time-of-flight secondary ion mass spectrometry (TOF-SIMS) for element- and molecule-specific imaging. In material sciences TOF-SIMS is used in surface characterization of nanostructured materials.[11] TOF-SIMS analysis utilizes a technique where samples are bombarded with a focused, energetic ion beam that sputters atoms, clusters, or large molecules (up to 10 000 u) off the surface.[12,13] A fraction is ejected as ions and mass analyzed. Sensitivity, efficiency, and quantification can be significantly improved by the use of Laser-SNMS which is especially suitable for ultratrace-element analysis.[12,14] Here the sputtering and ionization are decoupled by applying laser beams to ionize the majority of sputtered neutral particles. Both techniques result in very high lateral resolution (down to 100 nm). However, with

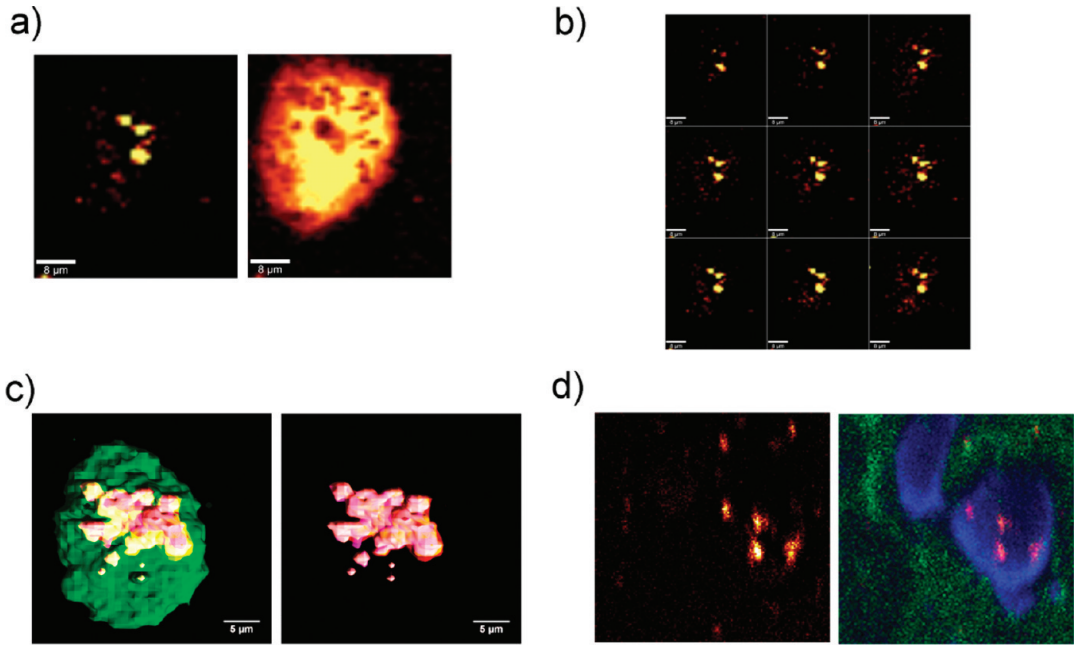

Figure 2. Confocal Raman microscopy and Laser-SNMS analysis of the uptake and intracellular location of peptide-coated 20 nm silver nanoparticles (Ag_{20}Pep) inside THP-1-derived macrophages. (a) Signals of intracellular Ag_{20}Pep particles and aggregates obtained by confocal Raman microscopy (incubation time, 24 h; exposure dose, 10 μg/mL); resolution, 1 μm × 1 μm × 0.5 μm; scale bar (white), 8 μm; single z-images displaying signals from nanoparticles only (left) or overlaid signals from intracellular organic matter and Ag_{20}Pep particles (same cell, right). (b) Complete confocal Raman microscopy scan showing signals of intracellular Ag_{20}Pep particles and aggregates (incubation time, 24 h; exposure dose, 10 μg/mL); resolution, 1 μm × 1 μm × 0.5 μm; scale bar (white), 8 μm; z-scan, start at +2.25 μm (upper left image) through −1.75 μm (lower right image). (c) 3D reconstruction of the sum of individual confocal Raman z-section planes; the silver signals are displayed in magenta and the cellular components in green; scale bar (white), 5 μm (3D animated videos are available in Supporting Information). (d) Laser-SNMS images of the silver isotope 106.9 u (left) and merged signals from sodium (green), carbon (blue), and silver (magenta); image area, 50 × 50 μm^2; total ion dose density, 4.5 × 10^{14} ions/cm^2.

TOF-SIMS high mass resolution cannot be obtained together with high lateral resolution. By using an additional sputtering ion beam to remove successive layers, a 3D image of the chemical composition of whole cells can be obtained—thus this technique is often called "chemical microscope". Since all ions can be recorded simultaneously, copious chemical information can be obtained that allows for cellular component identification and at the same time enables high-resolution imaging of both incorporated (exogenous) and physiological components inside single cells.[15]

The power of Laser-SNMS to image trace elements in cells and TOF-SIMS for molecular cellular analysis is demonstrated here for the first time to study nanosilver-mediated toxicity. The results are compared to the established confocal Raman microscopy and TEM and are supported through conventional biochemical assays.

RESULTS

Characteristic Features of the Nanoparticles Used. SNP of different sizes and coatings were synthesized as previously described.[9] They are covalently coated with a small peptide (Figure 1a,b). Here we used peptide-coated SNP of 20 nm (Ag_{20}Pep) or 40 nm (Ag_{40}Pep) diameter. Citrate-coated 20 nm SNP (Ag_{20}Cit) were used for comparison. We also included gold nanoparticles of same size and peptide coating (Au_{20}Pep) to serve as inert particle control. These particles enabled us to discriminate between rather unspecific and specific, silver-related nanoparticle effects. TEM images show that the peptide-coated particles are well-defined and uniform in size (Figure 1c). By contrast, citrate-coated particles are not as uniform, as being confirmed *via* polydispersity curves (Figure 1d) obtained from small-angle X-ray scattering (SAXS) analyses of suspensions in water (Supporting Information, Figure S1). The size distribution of Ag_{20}Pep particles is very narrow (polydispersity index of 0.18) but much broader for Ag_{20}Cit particles (polydispersity index of 0.38). First, useful subcytotoxic concentration ranges have been determined for all nanoparticles applied. If concentrations applied were considered on the basis of the particle's mass the smaller Ag_{20}Pep particles revealed stronger toxicity compared to larger Ag_{40}Pep particles (Supporting Information, Figure S2a). However, if doses were calculated on the basis of the particle's surface both types of particles displayed similar toxicity (Supporting Information, Figure S2b).

Visualization of SNP in Cells *via* Raman Microscopy and Laser-SNMS. Light microscopic inspection of cells after treatment revealed an uptake of nanoparticles and their intracellular aggregation over time (Supporting Information, Figure S2c). In addition, the peptide-coated SNP were traceable by confocal Raman microscopy due to covalent metal−sulfur and metal−amine bond stretching vibrations.[9] The signals obtained with this method can thus be

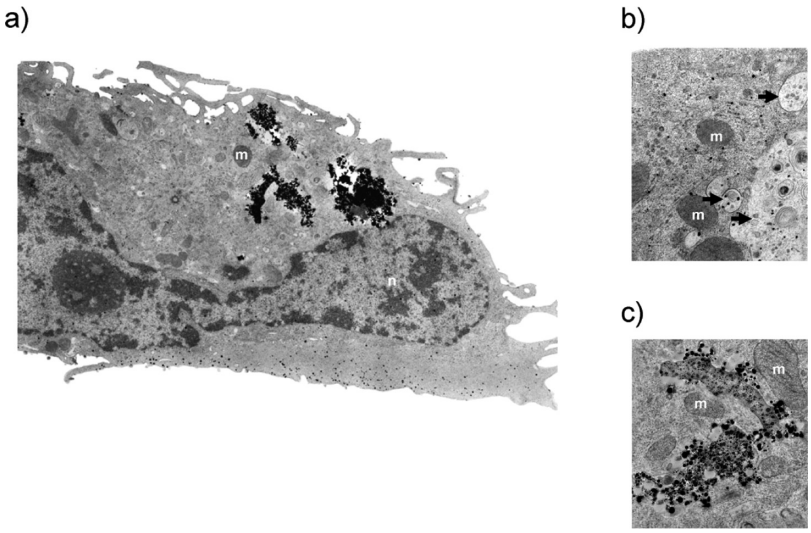

Figure 3. Transmission electron microscopy (TEM) of macrophage cells upon exposure to nanosilver. Representative ultrastructural image of one THP-1-derived macrophage cell treated with 20 μg/mL Ag_{20}Pep for 20 h. (a) Overview (magnification 5000×). (b) Detail showing lysosomes (indicated by black arrows) that contain nanosilver (magnification 31500×). (c) Detail on large intracellular aggregates of nanosilver (magnification 20000×): n, nucleus; m, mitochondrium.

considered specific for the coated nanoparticles, being undisturbed by any physiological components. Ag_{20}Pep particles easily get into macrophages (Figure 2a). A z-scan through individual cells (imaging of multiple section planes, plane resolution of 500 nm) proved silver aggregates are being trapped inside cells (Figure 2b). Besides three to five large clusters, many smaller aggregates are distributed throughout the intracellular space. An overlay of signals derived from both nanoparticles and total organic matter reveals that nanoparticles are indeed located inside cells (Figure 2a, compare left and right image). The 3D reconstruction of all individual layers recorded is shown in Figure 2c.

Application of Laser-SNMS/TOF-SIMS provides high quality images in terms of 2D and 3D resolution limits and sensitivity. Imaging of silver demonstrated significant accumulation of silver particles inside cells (Figure 2d, left image). Comparison of the spatial distribution of the phosphatidylcholine headgroup fragment $C_3H_8N^+$, a characteristic marker ion for cell membranes, with the spreading of Ag_{20}Pep particles revealed only few silver spots at the outer membrane (Supporting Information, Figure S3a.b, left). By contrast, analysis of the cells' interior compartments by sputtering through the membrane showed that the $C_3H_8N^+$ signal almost disappears while SNP concentrate at the inner side (Supporting Information, Figure S3a,b, right). These results confirmed the data obtained with confocal Raman microscopy, and both techniques unequivocally prove the presence of intracellular silver aggregates in different sizes (up to 5 μm cluster). Figure 2d (right image) displays an overlay of signals obtained with Laser-SNMS for extracellular sodium (green color), intracellular carbon (blue color), and intracellular silver (magenta color) at the single cell level.

Ultrastructural Analysis of SNP-Treated Macrophages *via* TEM. SNP-treated macrophages were analyzed by TEM to reveal ultrastructural details. Figure 3a illustrates a typical result obtained after treatment of THP-1-derived macrophages with 20 μg/mL Ag_{20}Pep for 20 h. Directly underneath the cell membrane high numbers of SNP are clearly visible, suggesting a rather nonselective uptake alongside the entire cell membrane. It further becomes obvious that a significant fraction of SNP is absorbed in nanoparticulate configuration, not as aggregates. The image also shows that SNP are distributed throughout the entire cell body either located freely dispersed in the cytoplasm, with no surrounding membranes embedding these particles, or located in cellular compartments such as lysosomes (Figure 3b) or even deep inside the nucleus. Conversely, SNP could not be detected within mitochondria or the endoplasmic reticulum. Only a few particles were occasionally seen attached to the outer membranes of these organelles, most likely by chance and not as result of specific target interactions. As with confocal Raman microscopy or Laser-SNMS, TEM visualizes extremely large aggregates within macrophages (Figure 3a). Inside these large clusters a fraction of SNP still strikes as single particles, well distinguishable from other individual species or from those contributing to differently sized aggregates (Figure 3c). TEM pictures of Ag_{40}Pep-treated macrophages reveal a very similar picture, whereas Ag_{20}Cit is taken up to a smaller extent and nanogold (Au_{20}Pep) is strongly incorporated but excluded from the nuclei (data not shown).

SNP-Mediated Alteration of Lipid Patterns in Cell Membranes of Macrophages. Next we used TOF-SIMS to study alterations in the lipid composition of the cytoplasmic

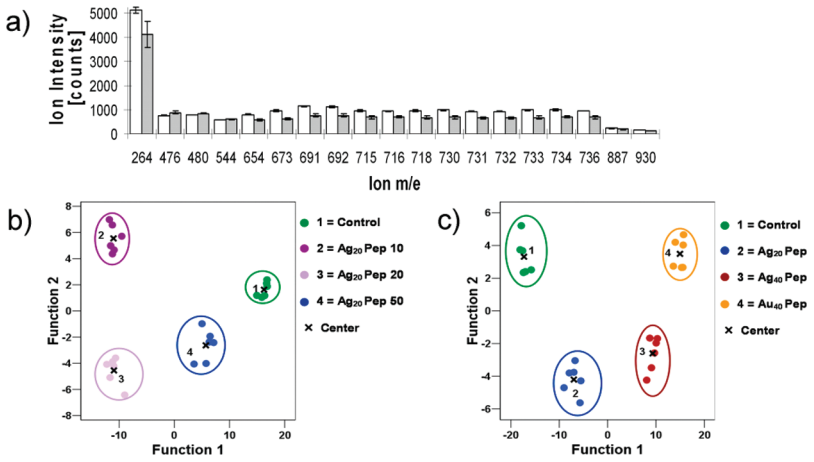

Figure 4. TOF-SIMS analysis of changes in lipid composition of cell membranes after nanoparticle treatment. (a) Histogram comparison of ion yields for 19 characteristic marker ions obtained after multivariate data reduction of six complete data sets of untreated (white bars) and treated cells (gray bars). Treatment conditions: 50 μg/mL Ag_{20}Pep and 24 h of incubation. (b) Values of the discriminant scores obtained from Fisher's discriminant analysis of 24 macrophage samples for 19 principal ions, which were selected to discriminate between cells treated with three different concentrations of Ag_{20}Pep (10, 20, and 50 μg/mL) and untreated macrophages. (c) Values of the discriminant scores obtained from Fisher's discriminant analysis of 24 macrophage samples for 34 principal ions, which were selected to discriminate between cells treated with 50 μg/mL Ag_{20}Pep, Ag_{40}Pep, or Au_{20}Pep each and untreated macrophages.

membrane outer leaflet of macrophages upon exposure to differently sized nanosilver (Ag_{20}Pep and Ag_{40}Pep) in comparison to nanogold (Au_{20}Pep). We also studied concentration-dependent effects of Ag_{20}Pep (10−50 μg/mL). Artifact creation was limited due to shock freezing. Raw spectral data were subjected to statistical analysis by focusing on the *m/z* range of 200−1000 (Figure 4). We compared six complete data sets of either untreated or SNP-treated cells. After data normalization and binning-like reduction, multivariate analyses of variance (MANOVA) and principal component analyses (PCA) were performed.[16] To show that the individual data sets could be separated from each other a Fisher's discriminant analysis was performed. As a result, 19 out of 800 single mass ions are found sufficient to separate macrophages treated with different concentrations of Ag_{20}Pep (Figure 4a,b). An additional set of 15 ions (total of 34 ions) then allows for further separation of cells treated with differently sized nanosilver and the identification of them from those treated with nanogold (Figure 4c). Supporting Information, Figure S4 provides a summary of the 34 marker ions identified and their chemical assignment according to the LIPID MAPS online tools database.[17] The structural assignment of 7 representative compounds out of these 19 phospholipid marker ions is given in Supporting Information, Figure S5.

SNP-Mediated Induction of Oxidative Stress in Macrophages. A closer look at the TOF-SIMS data on membrane lipid changes after treatment with SNP (Ag_{20}Pep, 50 μg/mL) reveals that contents of related lipid pairs (*i.e.*, lyso *vs* nonlyso forms) changed in an opposing manner (Supporting Information, Figure S3c). For instance, upon SNP treatment membrane levels of lysophosphatidyl ethanolamine (lyso-PE) C18:3 increase while those of phosphatidyl ethanolamine (PE) C36:6 decrease, indicating a loss of a C18:3 fatty acid side chain. The pair lysophosphatidyl choline (lyso-PC) C20:4/phosphatidyl choline (PC) C42:4 alters in the same way, thus indicating a loss of a C22:0 fatty acid side chain. Both changes are highly significant ($p < 0.01$). Intriguingly, the lyso-PC/PC ratio is a known indicator of inflammation and oxidative stress[18] which becomes increased during pathological processes such as Alzheimer's disease.[19] In addition, SNP treatment also increases the membrane levels of ceramides, a well-known marker of oxidative stress for years.[19]

We further supported our TOF-SIMS data by demonstrating intracellular oxidative stress *via* biochemical assays. SNP-dependent increases in protein carbonyl levels and the induction of heme oxygenase-1 (HO-1) are shown in Figure 5. Oxidative stress can be described as a tiered reaction resulting from disturbed cellular redox homeostasis due to the production of reactive oxygen species (ROS). Upon sensing of oxidative stress *via* the Nrf2/Keap1 system, cells upregulate levels of cytoprotective enzymes such as HO-1.[20]

Roughly 50−70% of all ROS generated in cells are scavenged by proteins.[21] Carbonyl moieties are among the most abundant reaction products thus representing a very sensitive measure of oxidative stress. We detected rapid formation of protein carbonyls (Figures 5a,b). Ag_{20}Pep caused higher levels of protein carbonylation when compared to Ag_{40}Pep, while nanogold (Au_{20}Pep) had only little effects. Interestingly, lower doses (*e.g.*, 20 μg/mL) were found more efficient in protein carbonyl formation than higher doses of nanoparticles (*e.g.*, 50 μg/mL).

Strong induction of HO-1 in macrophages after SNP treatment is shown in Figure 5c,d. The induction was

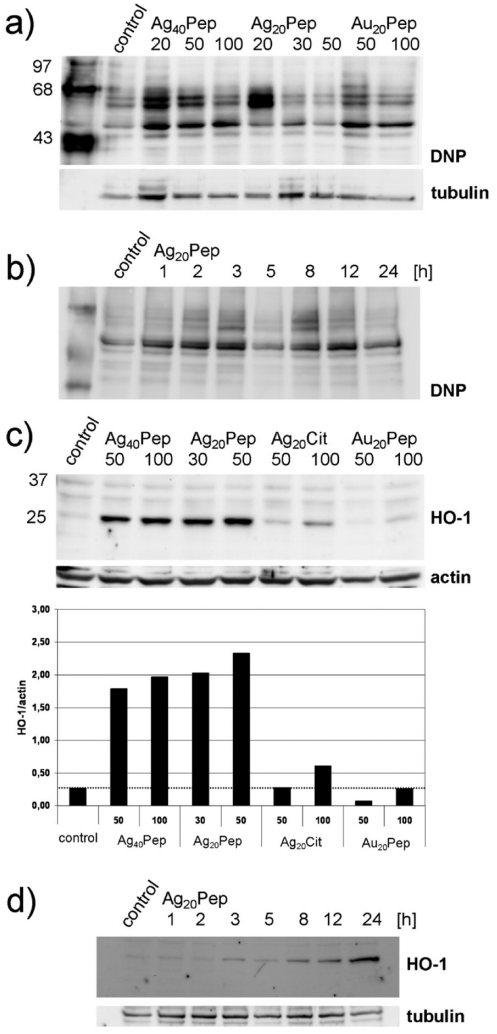

Figure 5. Generation of oxidative stress in macrophages by nanosilver. (a) Particle- and dose-dependent formation of protein carbonyls in macrophages. Detection of 2,4-dinitrophenyl hydrazone (DNP)-protein carbonyl adducts *via* immunoblot (OxyBlot Kit); doses are given in μg/mL; cells were exposed for 24 h. (b) Time-dependent formation of protein carbonyls in macrophages treated with Ag_{20}Pep particles: incubation times, 1−24 h; dose, 20 μg/mL. (c) Particle- and dose-dependent induction of heme oxygenase-1 (HO-1) expression in macrophages at 24 h of exposure; doses are given in μg/mL. Normalization of HO-1 protein expression (relative to actin signal) is shown in the lower graph. (d) Time-dependent induction of HO-1 expression in macrophages treated with Ag_{20}Pep particles: incubation times, 1−24 h; dose, 20 μg/mL.

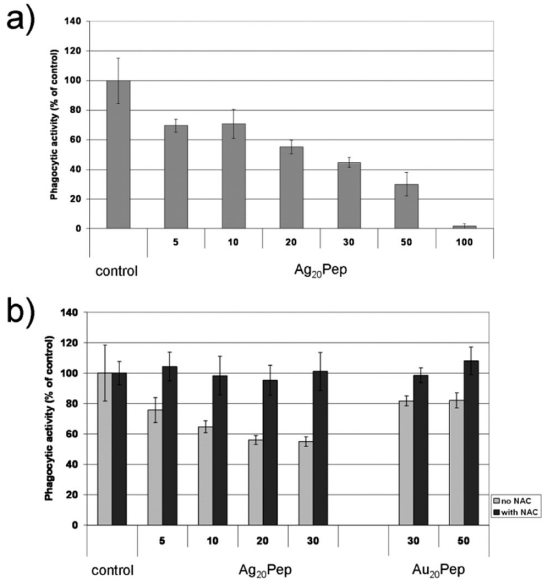

Figure 6. Functional impairment of macrophages due to nanosilver treatment. (a) Dose-dependent impairment of phagocytosis of cells treated with different concentrations (0−100 μg/mL) of Ag_{20}Pep for 24 h. (b) Prevention of dose-dependent disturbance of phagocytosis by pretreatment of macrophages with 5 mM *N*-acetylcysteine (NAC) for 5 h before particles were added (particle doses are given in μg/mL). Gold particles of 20 nm (Au_{20}Pep) served as inert control. Values in panels a and b are presented as percent phagocytosis compared to control: light bars, no pretreatment; dark bars, with pretreatment.

first detected after 3−5 h and then constantly increased for at least 24 h. In compliance with its cytotoxic potency, smaller particles (Ag_{20}Pep, IC_{50} = 110 μg/mL) caused stronger effects than larger particles (Ag_{40}Pep, IC_{50} = 140 μg/mL) when compared at mass doses. Ag_{20}Cit particles were barely cytotoxic and only weakly induced HO-1 at the highest concentration (100 μg/mL). Noncytotoxic nanogold did not affect HO-1 levels at all. Quantification of particle-induced HO-1 induction (Figure 5c) thus mirrors cell viability data (Supporting Information, Figure S2a). Intriguingly, the changes of the levels of ceramides, as obtained by TOF-SIMS, also reflect the same order. Here, treatment with smaller Ag_{20}Pep particles caused elevated levels of ceramides C30:2 and C36:4, while Ag_{40}Pep particles did not (Supporting Information, Figure S3c).

SNP-Mediated Functional Impairment of Macrophages. Since the lipid composition of cell membranes was significantly affected, we addressed the functionality of macrophages by studying its phagocytic activity. A dose-dependent impairment of phagocytosis was observed in cells treated with SNP (Figure 6). Even very low concentrations of Ag_{20}Pep particles exert drastic effects, while corresponding Au_{20}Pep particles are noneffective. With effective concentrations as low as 5 μg/mL Ag_{20}Pep the functional end point phagocytosis revealed most sensitive in our study. Dose-dependent disturbance of phagocytosis could be completely prevented by pretreatment of macrophages with the antioxidant *N*-acetylcysteine (NAC; Figure 6b). Thus, our results support literature data connecting oxidative stress in macrophages with impaired functional activity.[22]

DISCUSSION

Here we established a novel Laser-SNMS/TOF-SIMS approach to analyze human macrophages upon exposure to nanosilver and to compare this new method with two commonly applied and well established analytical methods, TEM and confocal Raman microscopy. All three

methods revealed very large aggregates within macrophages after treatment with SNP, thus indicating phagocytized aggregated material. In TEM images many individual particles were detectable throughout the cell's interior, but particularly directly underneath the cell membrane suggesting a nonphagocytotic uptake of individual particles.

With respect to all three methods applied, confocal Raman microscopy is fastest, allows for 3D reconstruction of cells, and does not require extensive sample preparation. With Laser-SNMS, however, images of particles inside cells could be recorded in much greater quality in terms of 3D resolution limits and sensitivity. In general, Laser-SNMS is capable of detecting metal atoms with a spatial resolution of down to 100 nm.[23] Thus, with this new approach we obtained much better lateral resolution compared to confocal Raman microscopy (400−500 nm).

On the other hand, TOF-SIMS alone usually is not sensitive enough for such purposes.[24] TOF-SIMS is, however, highly suitable to detect and image, for instance, lipid changes in cell membranes. Basically all molecular layers of individual cells can be analyzed, and after 3D reconstruction quantification is possible. Applying TOF-SIMS we found significant alterations in the membrane lipid patterns of macrophages upon treatment with SNP. The increase in ceramides in SNP-treated cells is characteristic for stress/inflammation conditions and indicates higher sphingomyelinase activity. Sphingomyelin is organized in microdomains (lipid rafts) almost exclusively on the outer leaflet of the cell membrane.[25] Ceramide formation causes a general redistribution. It equally distributes between the outer and inner leaflet and spontaneously fuses into large platforms, bringing together and thus activating otherwise inactive monomeric signaling proteins. Lipid rafts in untreated cells and ceramide-enriched membrane platforms in treated cells are recognition sites for different signaling molecules. The toll-like receptor 4 only translocates to sphingomyeline-enriched lipid rafts in the plasma membrane of macrophages,[26] while signaling molecules like CD95, CD28, CD5, LFA-1, interleukin-1 receptor, and PAF allocate to ceramide-enriched membrane platforms.[27] Alteration of signaling pathways in cells upon nanosilver treatment therefore becomes very likely. Here we can associate for the first time specific ceramides (C30:2 and C36:4) with these changes. The ceramide C36:4 is reconstructed from the ceramide fragment C18:3 and the ceramide headgroup N−C18:1, which is present in all ceramides in human macrophages.

In untreated cells higher amounts of phosphatidyl ethanolamines (PE) and phosphatidyl cholines (PC) are found while after treatment the corresponding lysophospholipid levels are elevated. The PC/lyso-PC pairs are of special interest since changes will directly affect membrane fluidity and several signaling cascades. Phospholipase A_2 seems activated after treatment, and such an increased activity has been linked to membrane ruffling and increased pinocytosis;[28] Lyso-PC favors micellar structures in the cell membrane, inhibits the flip-flop mechanism,[29] thus changing membrane fluidity and ultimately may lead to spontaneous rupture of the cell membranes *via* "hole formation". ABC transporters contribute to transmembrane transport processes such as pinocytosis of a wide variety of substrates and a large number of metabolites in macrophage cells.[30] ABC knockout mice show a significant different phospholipid content.[31] Interestingly the phosphatidyl cholines PC32:0 (*m/e* 734), PC32:1 (*m/e* 732), PC32:2 (*m/e* 730), as well as the phosphatidyl ethanolamine PE36:6 (*m/e* 736), are found significantly reduced in SNP-treated macrophages (Figure 4 and Supporting Information, Figure S4), and thus may indicate alterations at the ABC transporter level.

The particle uptake of macrophages occurs very fast, detectable within minutes. The load of nanoparticles incorporated within a 2-h period results in similar levels of cytotoxicity when compared to a continuous 24-h treatment, thereby suggesting particle-mediated effect saturation at high treatment doses (50 μg/mL) in short time (Supporting Information, Figure S7). Protein carbonyl formation is detected after 1 h as first response indicating the formation of a constant but low level of ROS, rather than sudden ROS bursts. Only later, with slower kinetics, are cytoprotective systems switched on and HO-1 induction appears (3−5 h). Oxidative stress might also trigger the observed lipid changes which are likely to occur in parallel with functional impairment of cells. With recovery experiments (Supporting Information, Figure S7) we can distinguish three differently effective concentration ranges for Ag_{20}Pep particles. At very high concentrations (≥50 μg/mL) macrophages die rapidly due to strong particle-mediated cytotoxicity. Medium concentrations (10−30 μg/mL) lack acute cytotoxicity within the first 24 h but cause strong oxidative stress responses, lipid changes, and functional impairment. Eventually cells perish as well. At doses below 10 μg/mL cells are only marginally impaired and may recover. On the basis of our results we propose a "dose of no return" of 10 μg/mL SNP. This corresponds to approximately 70−100 pg of silver per cell and thus is in a comparable range to the overload dose determined from *in vivo* studies (20 pg per single cell).[32]

CONCLUSION

A novel Laser-SNMS/TOF-SIMS approach was introduced to visualize nanoparticles inside human cells and to follow subtle biochemical alterations related to nanoparticle treatment. Through comparison with established methods such as confocal Raman microscopy and TEM, we proved the exceptional advantages of the new

method. Laser-SNMS turned out to afford highest spatial resolution in visualizing unlabeled silver nanoparticles. TOF-SIMS proved excellent to decipher and pinpoint complex biochemical changes in lipid membrane layers of cells upon treatment with nanosilver. Together Laser-SNMS/TOF-SIMS allows for imaging ultratrace element concentrations within nanometer-scale resolution and upper *part-per-billion* sensitivity in cells in cultures.

MATERIALS AND METHODS

Synthesis of Nanoparticles. Chemicals were obtained in p.a. quality from Bachem (Bubendorf, Switzerland) or Fluka (Buchs, Switzerland). All amino acids were L isomers. The peptide and SNP were prepared as published[9] and purified by repeated centrifugation−redispersion prior to freeze-drying. In the experiments we used peptide-coated SNP of 20 nm (Ag_{20}Pep) and 40 nm (Ag_{40}Pep) diameter and, 20 nm citrate-coated silver (Ag_{20}Cit) or peptide-coated gold (Au_{20}Pep) nanoparticles for comparison. Au_{20}Pep nanoparticles were prepared *via* ligand exchange of citrate-coated gold nanoparticles.

Characterization of Nanoparticles. Characterization data are summarized in Figure 1 and in Supporting Information, Figure S1. After synthesis particles were characterized by several methods. TEM images were taken at an FEI Morgani 268D operated at 80 kV. Samples were deposited on carbon-coated copper grids and directly imaged after drying on air. Some samples were diluted prior to imaging to allow for better imaging conditions. SAXS measurements were performed with a SAXSess camera (Anton Paar, Austria) attached to a laboratory X-ray generator (PW3830, PANanalytical) operated with a fine focus glass X-ray tube at 40 kV and 50 mA (Cu Kα, $\lambda = 0.1542$ nm). Samples were filled in a reusable vacuum tight 1 mm quartz capillary to attain the same scattering volume and background contribution. Data were analyzed as published elsewhere.[9] Size distributions were analyzed *via* dynamic light scattering at room temperature with a Zetasizer ZS (Malvern Instruments, UK). Particles were dispersed in distilled water or in cell culture medium, and samples were not filtered. The laser wavelength was 633 nm, and data were recorded in a backscattering mode at $2\theta = 173°$. Optical properties of bulk metallic silver and gold were used for data analysis.[33] In addition particles' chemical composition and crystallinity were determined (data not shown). The particles were found free of endotoxins as assessed by LAL endotoxin kit (Lonza, Germany).

Suspension of Nanoparticles. Nanoparticle aliquots were stored freeze-dried at −80 °C. Suspensions of particles were freshly prepared before each experiment. Aliquots of SNP were first resuspended in acidified water with ultrasonication and then diluted in cell culture medium.

Cell Culture. THP-1 cells were cultured in RPMI 1640 medium supplemented with 10% fetal bovine serum, 2 mM L-glutamine, 100 U/mL penicillin, 100 μg/mL streptomycin, 10 mM Hepes, and 1 mM sodium pyruvate. A 100 ng/mL concentration of phorbol-12-myristate-13-acetate (PMA) was used to differentiate THP-1 cells into macrophages during a time period of 24−48 h.[34] Cells changed morphology during differentiation. To characterize the differentiated macrophages we tested cellular responses such as TNF-α secretion after treatment with lipopolysaccharide (LPS) *via* enzyme-linked immunosorbent assay.[34]

WST-1 Cell Viability Assay. Cells were differentiated in 96-well culture plates for 24 h and treated with nanoparticles for 24−48 h. WST-1 reagent was purchased from Roche Diagnostics (Mannheim, Germany). Spectrophotometric read-out was performed 3 h after adding the WST-1 reagent with supernatants only. Interfering nanoparticles were removed in a table top centrifuge by centrifugation with maximum speed. In an alternative (cytoprotection) assay cells were pretreated with 5 mM of the antioxidant *N*-acetylcysteine (NAC) for 5 h before nanoparticle suspensions were added. In cell recovery assays the cells were carefully washed with PBS three times after indicated incubation time. Then fresh medium was added and cells were allowed to recover for different time periods before being assessed with WST-1 assay.

Fluorescence-Activated Cell Sorting (FACS) Analysis. For FACS analysis cells were grown in 24-well dishes, treated with indicated amounts of nanoparticles for the time periods indicated. Cells were washed three times and detached by accutase treatment. Staining was performed with annexin V and propidium iodide as published elsewhere.[35] FACS analysis was performed with a BD FACS CantoII (BD Biosciences, Heidelberg, Germany).

Confocal Raman Spectroscopy. After fixation with 4% paraformaldehyde cells were investigated with a confocal Raman microscope (CRM300, WITec, Ulm, Germany) equipped with a piezo-scanner (P-500, Physik Instrumente, Karlsruhe, Germany), a 60× objective, and a 532 nm Nd:YAG laser. Spectra were acquired with an air-cooled CCD detector (DU401-BV, Andor, UK) with 600 gratings/mm (UHTS 300, WITec, Germany). ScanCtrlSpectroscopyPlus (version 2.04, WITec) was used for data acquisition and processing. Power was adjusted to provide a good signal-to-noise ratio and to avoid sample destruction. Typically, less than 1 mW full beam power was applied at the sample. 3D reconstruction was performed using ImageJ 1.41, Image Magick 6.0-Q16 and VolumeJ 1.7a.

Laser-SNMS/TOF-SIMS Analyses. A dedicated cryogenic sample preparation technique with a high cooling rate was used for sample analysis.[13] Liquid propane was cooled down using liquid nitrogen, thus preventing evaporation of propane at the contact surface of the immersed specimen. This allowed accelerated cooling rates of up to 10^4 K/s on the surface of the sample. A combined reflectron-based Laser-SNMS/TOF-SIMS instrument with a mass resolution of approximately 2500 for Laser-SNMS and 6000 for TOF-SIMS was used for mass spectrometry analysis. For mass spectrometric analyses a pulsed, 25-keV, Bi_3^+ liquid metal ion gun (direct current (dc), 16 nA) was used to sputter material from the surface of the sample (total ion dose density for obtaining an image = 10^{13}−10^{14} ions/cm^2). A focused excimer laser beam (wavelength, 193 nm; repetition rate, 50 Hz; pulse width, 10 ns; pulse energy, 35 mJ; spot size diameter, 420 × 150 μm^2) was used to photoionize the sputtered neutral particles. Laser-SNMS spectra were recorded by scanning the primary ion beam over the analysis area, acquiring at each position mass spectra of all postionized secondary neutrals. For imaging of the lateral distribution of atoms and molecules, the intensities of the mass peaks in the spectra were calculated for each pixel of the rastered sample area and visualized with an intensity scale. The recorded data allow for imaging the distribution of every peak in the mass range of the analysis.

Statistics. The statistical analysis was performed as described in detail elsewhere.[16] In brief the acquired data were binned to 1 u. Data processing was carried out with the statistical package SPSS+ (version 12.0.2G) using the mass range between 200 and 1000 mass units to detect significant differences between untreated and SNP-treated cells. Ions lower than mass 200 were excluded from the study to avoid contaminating ions from salts, system contaminants, and other medium components. Each acquired spectrum was then normalized, setting the peak sum to 100%. For ion selection, a MANOVA was performed using the two data sets. All ions that showed 99.9% or higher variance differences were selected for multivariate analysis. To obtain a set of significant different ions being sufficient to discriminate between the two data sets, data reduction was performed as described elsewhere.[16] A first PCA was performed using all ions from the MANOVA. For data reduction a second PCA was performed with all ions from the first PCA, which loaded higher than 0.996 on factor 1 of the first PCA. This method was used for two PCA sets, one where different concentrations of Ag_{20}Pep

particles were tested, and one where different SNP and nanogold were compared. To show that data sets could be separated with a supervised model from each other a Fisher's discriminant analysis was performed using five factors for the Ag_{20}Pep samples, applied in different concentrations (representing 99.3% of the overall observed variance) and four factors (representing 98.8% of the observed variance) resulting from the second PCA. For both discriminant analyses the first two factors accounted for 98.8% of the observed variance in the model. The performance of the discriminant model was verified by applying the cross-validation procedure based on the "leave-one-out" cross-validation formalism.

TEM Analysis. TEM analysis was performed as previously described.[36] Cells in the culture dish were washed with phosphate buffered saline (PBS) and fixed overnight by immersion with Karnovsky's fixative at 4°C. After three washes in 0.1 M cacodylate buffer, postfixation was performed with 2% osmium tetroxide in 0.1 M cacodylate buffer for 1 h at 4 °C. After another three washes in 0.1 M cacodylate buffer, cells were removed from the culture dish and centrifuged at 2000*g* for 5 min. The pellet was then coated with 1.5% agar (Merck Eurolab, Darmstadt, Germany) for 30 min at 4°C. Subsequently the agar with the attached cell layer was removed from the wells. The samples were dehydrated in an ascending ethanol series (30−100% alcohol v/v) and embedded in Epon using beem capsules (Plano, Marburg, Germany). Polymerization was carried out at 60 °C for 24 h. Semithin sections (1 μm) were cut on an Ultracut E ultramicrotome (Reichert-Jung, Vienna, Austria) with a diamond knife, stained as published elsewhere,[36] and analyzed by light microscopy. Ultrathin sections (60 nm) were cut with a diamond knife, mounted on copper grids (Plano, Marburg, Germany) and examined with a Zeiss 10CR electron microscope (Jena, Germany).

Cell Lysates, SDS-PAGE, Immunoblot and Detection of Protein Carbonyls. Cells were washed with PBS three times and lysed by adding a modified RIPA buffer (50 mM Tris/HCl pH 7.4; 150 mM NaCl, 1 mM EDTA, 1% Igepal, 0.25% Na-deoxycholate). Lysates were centrifuged and stored at −80 °C. Protein concentrations were determined through Bradford assay (BioRad, München, Germany), and SDS-PAGE was performed according to standard protocols. SDS-PAGE gels were transferred onto nitrocellulose membranes with a semidry blotting system. For detection of protein carbonyls OxyBlot Kit (Millipore, Schwalbach, Germany) was used. Antibodies against HO-1, tubulin, or actin were obtained from Abcam (Abcam, Cambridge, UK). Images were obtained with GelDoc system (BioRad, München, Germany) and analyzed with QuantityOne software.

Phagocytosis Assay. For phagocytosis, THP-1 cells were differentiated into macrophages in a 96-well format. Cells were then treated with nanoparticle suspensions for 24 h. After treatment phagocytotic activity was analyzed by applying the phagocytosis assay (Invitrogen, Darmstadt, Germany) according to manufacturer's instructions.

Acknowledgment. The authors acknowledge excellent technical assistance of Annika-Mareike Gramatke, Antje Bergert, Doreen Wittke, and Monika Sachtleben. A. Mantion thanks the Adolf-Martens e.V. for an Adolf-Martens Fellowship. A. Masic is grateful for support by the Alexander von Humboldt Foundation and the Max-Planck-Society in the framework of the Max-Planck Research Award by the Federal Ministry of Education and Research. Financial support by the Federal Institute of Risk Assessment (BfR), the Federal Institute for Materials Research and Testing (BAM), the Swiss National Science Foundation, the NCCR Nanoscience, the University of Potsdam, the Free University of Berlin, the Fond der Chemischen Industrie, and the MPI of Colloids and Interfaces (Colloid Chemistry Department) is gratefully acknowledged.

Supporting Information Available: Figure S1: Characterization data of citrate- and peptide-coated nanoparticles. Figure S2: Dose-, time- and size-dependent toxicity of different nanoparticles on macrophages in culture. Figure S3: Laser-SNMS analysis of the uptake and intracellular location of silver nanoparticles inside THP-1-derived macrophages and TOF-SIMS mass spectra evaluation. Figure S4: Summary of the characteristic marker ions used for separation. Figure S5: Structural assignment of characteristic molecular marker ions obtained by TOF-SIMS analysis of nanosilver-treated macrophages. Figure S6: Quantification of the fraction of apoptotic *vs* necrotic macrophages upon treatment with nanoparticles. Figure S7: Recovery experiments after treatment of macrophages with peptide-coated 20 nm silver nanoparticles (Ag_{20}Pep). In addition two animated 3D movies from Confocal Raman Microscopy. This material is available free of charge *via* the Internet at http://pubs.acs.org.

REFERENCES AND NOTES

1. Chen, X.; Schluesener, H. J. Nanosilver: A Nanoproduct in Medical Application. *Toxicol. Lett.* **2008,** *176*, 1–12.
2. Xia, T.; Li, N.; Nel, A. E. Potential Health Impact of Nanoparticles. *Annu. Rev. Public Health* **2009,** *30*, 137–150.
3. Filipe, P.; Silva, J. N.; Silva, R.; Cime de Castro, J. L.; Marques Gomes, M.; Alves, L. C.; Santus, R.; Pinheiro, T. *Stratum Corneum* Is an Effective Barrier to TiO_2 and ZnO Nanoparticle Percutaneous Absorption. *Skin Pharmacol. Physiol.* **2009,** *22*, 266–275.
4. Larese, F. F.; D'Agostin, F.; Crosera, M.; Adami, G.; Renzi, N.; Bovenzi, M.; Maina, G. Human Skin Penetration of Silver Nanoparticles through Intact and Damaged Skin. *Toxicology* **2009,** *255*, 33–37.
5. Ji, J. H.; Jung, J. H.; Kim, S. S.; Yoon, J. U.; Park, J. D.; Choi, B. S.; Chung, Y. H.; Kwon, I. H.; Jeong, J.; Han, B. S.; *et al.* Twenty-Eight-Day Inhalation Toxicity Study of Silver Nanoparticles in Sprague−Dawley Rats. *Inhal. Toxicol.* **2007,** *19*, 857–871.
6. Arora, S.; Jain, J.; Rajwade, J. M.; Paknikar, K. M. Cellular Responses Induced by Silver Nanoparticles: *In Vitro* Studies. *Toxicol. Lett.* **2008,** *179*, 93–100.
7. Jiang, W.; Kim, B. Y. S.; Rutka, J. T.; Chan, W. C. W. Nanoparticle-Mediated Cellular Response Is Size-Dependent. *Nat. Nanotechnol.* **2008,** *3*, 145–150.
8. Dickerson, M. B.; Sandhage, K. H.; Naik, R. R. Protein- and Peptide-Directed Syntheses of Inorganic Materials. *Chem. Rev.* **2008,** *108*, 4935–4978.
9. Graf, P.; Mantion, A.; Foelske, A.; Shkilnyy, A.; Masic, A.; Thünemann, A. F.; Taubert, A. Peptide-Coated Silver Nanoparticles: Synthesis, Surface Chemistry, and pH-Triggered, Reversible Assembly into Particle Assemblies. *Chem.—Eur. J.* **2009,** *15*, 5831–5844.
10. Mühlfeld, C.; Rothen-Rutishauser, B.; Vanhecke, D.; Blank, F.; Gehr, P.; Ochs, M. Visualization and Quantitative Analysis of Nanoparticles in the Respiratory Tract by Transmission Electron Microscopy. *Part. Fibre Toxicol.* **2007,** *4*, 11–28.
11. Baer, D. R.; Gaspar, D. J.; Nachimuthu, P.; Techane, S. D.; Castner, D. G. Application of Surface Chemical Analysis Tools for Characterization of Nanoparticles. *Anal. Bioanal. Chem.* **2010,** *396*, 983–1002.
12. Arlinghaus, H. F. Possibilities and Limitations of High-Resolution Mass Spectrometry in Life Sciences. *Appl. Surf. Sci.* **2008,** *255*, 1058–1063.
13. Vickerman, J. C.; Gilmore, I. S. *Surface Analysis—The Principle Techniques*, 2nd ed.; Vickerman, J. C., Gilmore, I., Eds.; John Wiley & Sons: Chichester, UK, 2009.
14. Arlinghaus, H. F.; Kriegeskotte, C.; Fartmann, A.; Wittig, A.; Sauerwein, W.; Lipinsky, D. Mass Spectrometric Characterization of Elements and Molecules in Cell Cultures and Tissues. *Appl. Surf. Sci.* **2006,** *252*, 6941–6948.
15. Ostrowski, S. G.; van Bell, C. T.; Winograd, N.; Ewing, A. G. Mass Spectrometric Imaging of Highly Curved Membranes during *Tetrahymena Mating*. *Science* **2004,** *305*, 71–73.
16. Jungnickel, H.; Jones, E. A.; Lockyer, N. P.; Oliver, S. G.; Stephens, G. M.; Vickerman, J. C. Application of ToF-SIMS with Chemometrics to Discriminate Between Four Different Yeast Strains from the Species *Candida glabrata* and *Saccharomyces cerevisiae*. *Anal. Chem.* **2005,** *77*, 1740–1745.
17. Fahy, E.; Sud, M.; Cotter, D.; Subramaniam, S. LIPID MAPS Online Tools for Lipid Research. *Nucleic Acid Res.* **2007,** *35*, W606–W612.

18. Colles, S. M.; Chisolm, G. M. Lysophosphatidylcholine-Induced Cellular Injury in Cultured Fibroblasts Involves Oxidative Events. *J. Lipid Res.* **2000,** *41*, 1188–1198.
19. Cutler, R. G.; Kelly, J.; Storie, K.; Pedersen, W. A.; Tammara, A.; Hatanpaa, K.; Troncoso, J. C.; Mattson, M. P. Involvement of Oxidative Stress-Induced Abnormalities in Ceramide and Cholesterol Metabolism in Brain Aging and Alzheimer's Disease. *Proc. Natl. Acad. Sci. U.S.A.* **2004,** *101*, 2070–2075.
20. Xia, T.; Koyochich, M.; Brant, J.; Hotze, M.; Sempf, J.; Oberley, T.; Sioutas, C.; Yeh, J. L.; Wiesner, M. R.; Nel, A. E. Comparison of the Abilities of Ambient and Manufactured Nanoparticles to Induce Cellular Toxicity According to an Oxidative Stress Paradigm. *Nano Lett.* **2006,** *6*, 1794–1807.
21. Dalle-Donne, I.; Carini, M.; Orioli, M.; Vistoli, G.; Regazzoni, L.; Colombo, G.; Rossi, R.; Milzani, A.; Aldini, G. Protein Carbonylation: 2,4-Dinitrophenylhydrazine Reacts with both Aldehydes/Ketones and Sulfenic Acids. *Free Radic. Biol. Med.* **2009,** *46*, 1411–1419.
22. Kirkham, P. Oxidative Stress and Macrophage Function: A Failure to Resolve the Inflammatory Response. *Biochem. Soc. Trans.* **2007,** *35*, 284–288.
23. Kriegeskotte, C.; Möller, J.; Lipinsky, D.; Wittig, A.; Sauerwein, W.; Haier, J.; Arlinghaus, H. F. Imaging of Atomic and Molecular Species in Tissue with Laser-SNMS for Pharmaceutical Studies. *Surf. Interface Anal.* **2006,** *38*, 121–125.
24. Kollmer, F.; Bourdos, N.; Kamischke, R.; Benninghoven, A. Nonresonant Laser-SNMS and TOF-SIMS Analysis of Sub-μm Structures. *Appl. Surf. Sci.* **2003,** *203−204*, 238–243.
25. Simons, K.; Ikonen, E. Functional Rafts in Cell Membranes. *Nature* **1997,** *387*, 569–572.
26. Powers, K. A.; Szászi, K.; Khadaroo, R. G.; Tawadros, P. S.; Marshall, J. C.; Kapus, A.; Rotstein, O. D. Oxidative Stress Generated by Hemorrhagic Shock Recruits Toll-like Receptor 4 to the Plasma Membrane in Macrophages. *J. Exp. Med.* **2006,** *203*, 1951–1961.
27. Hannun, Y. A.; Obeid, L. M. Principles of Bioactive Lipid Signalling: Lessons from Sphingolipids. *Nat. Rev. Mol. Cell Biol.* **2008,** *9*, 139–150.
28. Bar-Sagi, D.; Feramisco, J. R. Induction of Membrane Ruffling and Fluid-Phase Pinocytosis in Quiescent Fibroblasts by Ras Proteins. *Science* **1986,** *233*, 1061–1068.
29. Martin, C.; Requero, M. A.; Masin, J.; Konopasek, I.; Goñi, F. M.; Sebo, P.; Ostolaza, H. Membrane Restructuring by *Bordetella pertussis* Adenylate Cyclase Toxin, a Member of the RTX Toxin Family. *J. Bacteriol.* **2004,** *186*, 3760–3765.
30. Dean, M.; Hamon, Y.; Chimini, G. The Human ATP- Binding Cassette (ABC) Transporter Superfamily. *J. Lipid Res.* **2001,** *42*, 1007–1017.
31. Fitzgerald, M. L.; Xavier, R.; Haley, K. J.; Welti, R.; Gross, J. L.; Brown, C. E.; Zhuang, D. Z.; Bell, S. A.; Lu, N.; McKee, M.; *et al.* ABCA3 Inactivation in Mice Causes Respiratory Failure, Loss of Pulmonary Surfactant, and Depletion of Lung Phosphatidylglycerol. *J. Lip. Res.* **2007,** *48*, 621–632.
32. Pauluhn, J. Pulmonary Toxicity and Fate of Agglomerated 10 and 40 nm Aluminium Oxyhydroxides Following 4-Week Inhalation Exposure of Rats: Toxic Effects Are Determined by Agglomerated, Not Primary Particles Size. *Toxicol. Sci.* **2009,** *109*, 152–167.
33. Johnson, P. B.; Christy, R. W. Optical Constants of the Noble Metals. *Phys. Rev. B* **1972,** *6*, 4370–4379.
34. Park, E. K.; Jung, H. S.; Yang, H. I.; Yoo, M. C.; Kim, C.; Kim, K. S. Optimized THP-1 Differentiation Is Required for the Detection of Responses to Weak Stimuli. *Inflammation Res.* **2007,** *56*, 45–50.
35. Aubry, J. P.; Blaecke, A.; Lecoanet-Henchoz, S.; Jeannin, P.; Herbault, N.; Caron, G.; Moine, V.; Bonnefoy, J. Y. Annexin V Used for Measuring Apoptosis in the Early Events of Cellular Cytotoxicity. *Cytometry, Part A* **1999,** *37*, 197–204.
36. Richardson, K. C.; Jarett, L.; Finke, E. H. Embedding in Epoxy Resins for Ultrathin Sectioning in Electron Microscopy. *Stain. Technol.* **1960,** *35*, 313–323.